Correspondence to:
Y. Wang,
yuhang.wang@eas.gatech.edu

Author Contributions:
Conceptualization: Hang Qu, Yuhang Wang
Formal analysis: Hang Qu, Yuhang Wang
Methodology: Hang Qu, Ruixiong Zhang
Software: Hang Qu, Ruixiong Zhang
Validation: Hang Qu, Ruixiong Zhang, Jianfeng Li
Visualization: Hang Qu
Writing - original draft: Hang Qu, Yuhang Wang

Extending Ozone-Precursor Relationships in China From Peak Concentration to Peak Time

Hang Qu[1] [iD], **Yuhang Wang[1]** [iD], **Ruixiong Zhang[1]** [iD], and **Jianfeng Li[1]** [iD]

[1]School of Earth and Atmospheric Sciences, Georgia Institute of Technology, Atlanta, GA, USA

Abstract High ozone concentrations have become the major summertime air quality problem in China. Extensive in situ observations are deployed for developing strategies to effectively control the emissions of ozone precursors, that is, nitrogen oxides ($NO_X = NO + NO_2$) and volatile organic compounds (VOCs). The modeling analysis of in situ observations often makes uses of the dependence of ozone peak concentration on NO_X and VOC emissions, because ozone observations are among the most widely available air quality measurements. To extract more information from regulatory ozone observations, we extend the ozone-precursor relationship to ozone peak time in this study. We find that the sensitivities of ozone peak time and concentration are complementary for regions with large anthropogenic emissions such as China. The ozone peak time is sensitive to both VOC and NO_X emissions, and the sensitivity is nearly linear in the transition regime of ozone production compared to the changing ozone peak concentration sensitivity in this regime, making the diagnostics of ozone peak time particularly valuable. The extended ozone-precursor relationships can be readily applied to understand the effects on ozone by emission changes of NO_X and VOC and to assess potential biases of NO_X and VOC emission inventories. These observation constraints based on regulatory ozone observations can complement the other measurement and modeling analysis methods nicely. Furthermore, we suggest that the ozone peak time sensitivity we discussed here to be used as a model evaluation measure before the empirical kinetic modeling approach (EKMA) diagram is applied to understand the effectiveness of emission control on ozone concentrations.

Plain Language Summary High ozone concentrations have become the major summertime air quality problem in China. Air quality models are routinely used to investigate effective ozone strategies by controlling the emissions of ozone precursors, nitrogen oxides ($NO_X = NO + NO_2$) and volatile organic compounds (VOCs). Therefore, the evaluations of model-simulated sensitivities of ozone to its precursor emissions using available observations are urgently needed. In the past, efforts have been focused on sensitivities of ozone peak concentrations to its precursor emissions. We show in this work that the observations of ozone peak time can also be applied to understand ozone sensitivities to its precursor emissions, especially in regions with large anthropogenic emissions such as China. Before air quality models are applied to investigate effective strategies of controlling ozone precursor emissions, we suggest that the model simulations of ozone peak time and concentrations are evaluated using the extensive regulatory air quality monitoring network data. Model biases in simulated ozone peak time or concentrations also provide important clues to potential model errors, such as systematic biases in the estimated emissions of ozone precursors. These biases in model simulations can lead to erroneous emission control strategies and need to be corrected before air quality models can be used in policy applications.

1. Introduction

Ground-level ozone is a secondary air pollutant that damages human and vegetation health (U.S. EPA, 2013). The chemical production of ground-level ozone involves the photochemical reactions between nitrogen oxides ($NO_X = NO + NO_2$) and volatile organic compounds (VOCs) (Seinfeld & Pandis, 2016). The ozone-precursor relationship, that is, the sensitivity of ozone to NO_X and VOC emissions, is an important factor in establishing effective ozone control strategies (Blanchard & Fairley, 2001; Geng et al., 2008; Jimenez & Baldasano, 2004; Liu et al., 2012; Parra et al., 2009; Ren et al., 2013; Yang et al., 2011; Zhao et al., 2009). In China megacity clusters, ozone production is often in the transition regime (Jin & Holloway, 2015; Li et al., 2013; Liu et al., 2012; Ran et al., 2009; Xing et al., 2011).

China is experiencing high levels of ozone due to high precursor emissions in association with rapid urbanization and industrialization (Duncan et al., 2016; Lin et al., 2013; Ma et al., 2019; Sun et al., 2019; Wang et al., 2017; Zhao et al., 2013). In July 2018, for example, ozone was the dominant air pollutant in 155 of the 168 major cities in China, and in 104 of them, the maximum daily 8-hr average (MDA8) ozone exceeds 160 $\mu g\ m^{-3}$ (~80 ppbv, the Grade II national air quality standard of China) (CNEMC, 2018). Ozone has been increasing by 1–3 ppbv yr^{-1} in urban and background regions in China recently (Gao et al., 2017; K. Li et al., 2019; Ma et al., 2016). In this fast-changing environment, observation constraints are sorely needed on precursor emissions used in the model and model-based emission control strategies.

Diagnosing ozone sensitivity to precursor emissions often requires intensive field observations of a suite of chemical species (e.g., Liu et al., 2012; Lu et al., 2017). When the extensive field measurements are unavailable, it is often desirable to use the observations from the regulatory monitoring networks. The benefit is that these networks cover vast regions in a nation, but the limitation is that precursor measurements either have issues or are unavailable (e.g., J. Li et al., 2019). High-quality measurements of ozone are readily available from these networks (e.g., Lu et al., 2018). A commonly used ozone-precursor relationship is the dependence of peak concentration of daytime ozone on NO_X and VOC emissions, which is also known as the empirical kinetic modeling approach (EKMA) diagram (e.g., Ashok & Barrett, 2016; Kinosian, 1982; Tan et al., 2018). For regulatory application purposes, it is natural to focus on peak ozone concentrations. However, from the point of view of modeling diagnostics and making use of the extensive ozone observations from monitoring networks, ozone peak time is also of interest. Previous studies showed that the spatial and temporal distributions over the cities (Wang et al., 2017; Yang et al., 2020) and model simulations revealed that the peak time of the average diurnal profile of ozone responds to VOC or NO_X emissions (Karl et al., 2019; J. Li et al., 2019; Ojha et al., 2012).

In this study, we extend the ozone-precursor relationship to ozone peak time and investigate the potential of using extensive ozone observations in China to improve observation constraints on model simulated ozone-precursor relationships (J. Li et al., 2019). We use the observations of ozone in July 2014 as an example to demonstrate this potential. We show that ozone peak time's dependence on NO_X and VOC emissions offers new constraints on the emissions that are different from those placed by the observed peak concentrations. Therefore, the discrepancies between simulated and observed ozone peak time and peak concentrations can be applied to understand the biases in ozone precursor emission inventories and provide pertinent guidance on adjusting model-based emission control strategies.

2. Data and Methods

2.1. The China National Environmental Monitoring Center (CNEMC) Network

CNEMC has established ambient atmosphere quality monitoring networks across the country since 2013, reporting hourly real-time data of six criteria pollutants (O_3, CO, NO_2, SO_2, $PM_{2.5}$, and PM_{10}) and air quality index (AQI) in cities online (http://www.cnemc.cn). The data were used in recent studies for analyzing the current air quality issues (K. Li et al., 2019; Liu et al., 2018; Lu et al., 2018). In this work, we analyzed the hourly surface ozone observations from 861 sites in 189 cities for July 2014. For each site, we remove all the data that are higher than four times the monthly average of 3-hr running mean data for the hour of the observations. We then group the data by the hour of the observation and apply Tukey's fences to remove outliers. Specifically, we remove the outlier data which are outside the range of $Q_1 - k(Q_3 - Q_1)$ and $Q_3 + k(Q_3 - Q_1)$, where Q_1 and Q_3 are the 25th and 75th quartiles, respectively, and $k = 1.5$ (Tukey, 1977). A total of 2.3% of the measurement data are removed. Comparison with another data quality control method (Lu et al., 2018) and no data quality control shows that the regional mean ozone peak time and peak concentration values are insensitive to the quality control method used (Text S1 and Figures S1 and S2 in the supporting information). The results presented in this work change negligibly when all the observation data are used. For each city, processed hourly observation data are first averaged over all sites, and peak time and peak concentration of ozone are then calculated separately for each city in each day. The days with missing daytime (8 a.m. to 8 p.m. in local Sun time) hourly data are excluded in the peak value analysis. The peak time of ozone is converted to local Sun time based on the longitude of the city. If a computed daily peak time of ozone occurs at nighttime (8 p.m. to 8 a.m. in local Sun time), manual inspection is made either to discard the data or to recalculate the daytime ozone peaks for that day. The resulting daily data for each city are used

to compute regional averages. Model results for cities with corresponding observation data are processed in the same manner.

2.2. The 3-D Regional Chemical Transport Model

The 3-D Regional chEmical trAnsport Model (REAM) has been widely used in studies over North America, East Asia, and other regions (Gu et al., 2014; Liu, Wang, Vrekoussis, et al., 2012; Liu et al., 2014; Wang et al., 2006, 2007; Xu et al., 2018; Zeng et al., 2006; Zhang et al., 2016; R. Zhang et al., 2017, 2018; Zhao, Wang, Choi, et al., 2009). The horizontal resolution of the model is 36 km with 30 vertical layers in the troposphere. Meteorological data are obtained from the Weather Research and Forecasting model (WRF 3.6) assimilations constrained by the National Centers for Environmental Prediction Climate Forecast System Version 2 (NCEP CFSv2) products (Saha et al., 2013). The boundary conditions for chemical tracers are obtained from the GEOS-Chem model (v9–02) (Bey et al., 2001). The chemistry mechanism extends the GEOS-Chem chemistry mechanism with reactions involving aromatics, ethylene, and acetylene. The Multiresolution Emission Inventory for China (MEIC, http://www.meicmodel.org/) emissions for the year 2012 are adopted in the model for anthropogenic emissions of NO_X, VOCs, and CO (Li et al., 2017). The emissions are scaled by the diurnal ratio taken from the National Emissions Inventory (NEI), and there is no weekday-to-weekend variation. Biogenic emissions of isoprene are calculated using the Model of Emissions of Gases and Aerosols from Nature (MEGAN v2.1) (Guenther et al., 2012). We run the model for July 2014, the same period as the data we used. The model is spun up for 10 days for initialization.

A 0-D box model is also developed based on the 3-D REAM. The 0-D box model uses the same chemical mechanism as the 3-D REAM model. The meteorological, physical, and chemical parameters including temperature, pressure, water concentration, boundary layer height, photolysis rates, deposition rates, and aerosol surface area are averaged hourly for city grid cells with surface ozone observations. Advection transport is specified with a transport lifetime of 5.3 hr, corresponding to an average city scale of 100 km and an average wind speed of 5.2 m s^{-1}. Hourly background concentrations for ozone are set at the fifth percentile value of the observations. Hourly backgrounds of other chemical tracers are set at the fifth percentile values of 3-D REAM results. Each simulation is run until a steady state is reached when the differences in ozone peak concentration and time converge to <1% from the results of the previous day. A total of 400 simulations were conducted for NO_X emissions in the range of 0–4.5 × 10^{16} molecules m^{-2} s^{-1} and VOC emissions in the range of 0–1.4 × 10^{17} molecules m^{-2} s^{-1}; NO_X and VOC emissions are evenly divided into 20 bins each. The upper limits of NO_X and VOC emission ranges correspond to three times of average MEIC emissions for the cities with surface ozone observations.

3. Results

3.1. Correlations of O$_3$ Peak Concentration and Time to NO_X and VOC Emissions

The ozone-precursor relationships to be studied can be simply illustrated by the correspondence of ozone peak time and concentration to NO_X and VOC emissions in China. Figures 1a and 1b show the correlations between ozone peak concentration and NO_X and VOC emissions, respectively. The correlation coefficients of ozone peak concentration with NO_X and VOC emissions are comparable at 0.54 and 0.53, respectively. In small cities with NO_X emissions <1 × 10^{15} molecules m^{-2} s^{-1}, the transport processes dominate the concentrations of ozone and its precursors, and we remove these four sites (3%) of Beihai, Zhangjiajie, Weihai, and Lhasa to focus on the effects of local ozone photochemistry. Figure 1c shows that the observed ozone peak time correlates well with MEIC NO_X emission ($R = 0.61$) in the cities with strong NO_X emissions (>1 × 10^{15} molecules m^{-2} s^{-1}). The ozone peak time delays from 1–3 to 4–6 pm as the NO_X emissions increase from 1 × 10^{15} to 1 × 10^{17} molecules m^{-2} s^{-1}. The ozone peak time is also correlated with VOC emission with an R value of 0.56 (Figure 1d). Figure 1 implies that the EKMA-type relationship between ozone peak concentration and its precursor emissions may be extended to ozone peak concentration in China.

3.2. Modeling Analysis of the Observations

The observed and simulated distribution of maximum daily 8-hr average (MDA8) ozone concentrations in the cities are evaluated in Figure 2a. The mean simulated ozone concentration over the city grid cells is 57 ± 12 ppbv, which is comparable to the observed 53 ± 13 ppbv, with an overall correlation coefficient of 0.72. To understand regional characteristics, we grouped the data into six regions by economic
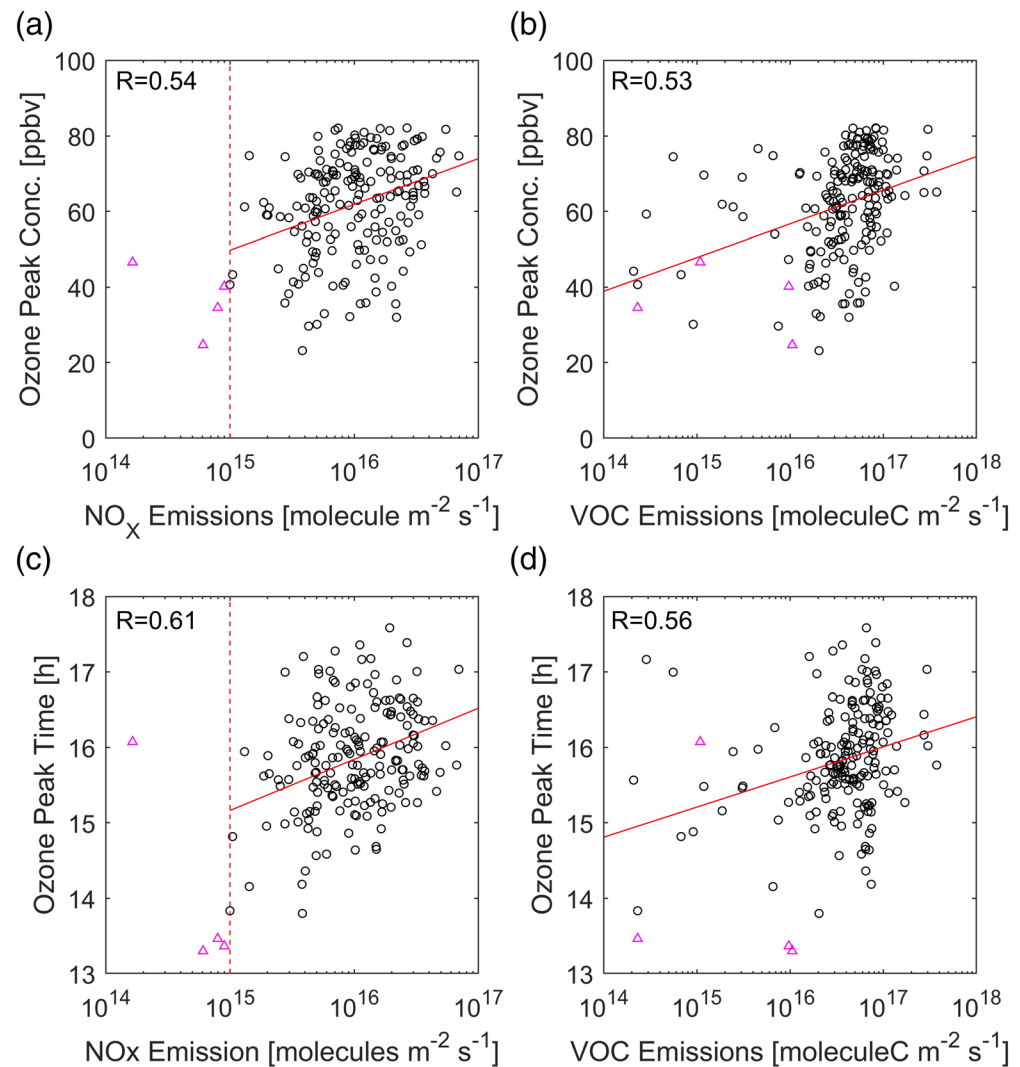
Figure 1. Observed ozone peak concentration and time as a function of NO_X and VOC emissions in the MEIC inventory, respectively, for July 2014. The pink triangles denote urban regions with NO_X emissions $<10^{15}$ molecules m^{-2} s^{-1}, which are excluded from this study. The red line is a least squares regression for urban regions with NO_X emissions $>10^{15}$ molecules m^{-2} s^{-1}.

development and topography (Figure 2b): North Central Plain (NCP), Northeast (NE) region, Yangtze River Delta (YRD), Northwest (NW) region, Southwest (SW) region, and Pearl River Delta (PRD). Table 1 summarizes the regional statistics. The observed mean MDA8 ozone concentrations range from 41 to 64 ppbv in the six regions. The highest mean ozone concentration occurs in the NCP region, and the lowest mean concentration occurs in the PRD region. The model results differ from the observations by 0–13 ppbv in the six regions, and the correlation coefficients between observed and simulated ozone range from 0.61 to 0.81.

The comparisons of the monthly means of the simulated and observed ozone peak concentration and peak time are illustrated in Figures 2c and 2d. Both the observed and simulated monthly mean ozone peak concentrations in the cities are in the range of 20–90 ppbv, and they are strongly correlated with a *R* value of 0.71. Most of the simulation results lie between the 1:2 and 2:1 lines with some exceptions in the SW and YRD regions, where the simulated peak ozone concentrations are overestimated. The ozone peak concentrations are highest in the NCP region and lowest in the PRD region. The observed and simulated ozone peak time data are moderately correlated with *R* = 0.51, and the range of the ozone peak time is mostly from 2 to
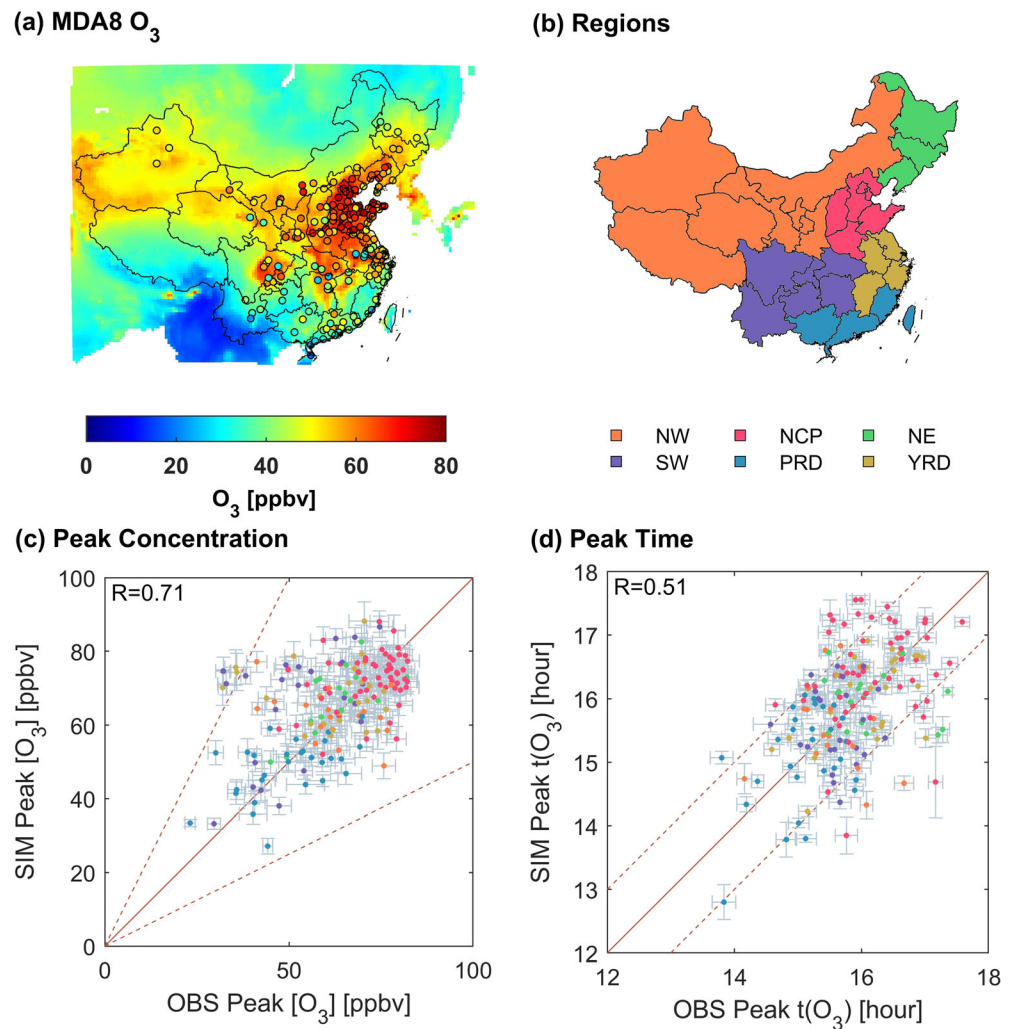
Figure 2. Panel (a) shows the simulated (background) and observed (circle) maximum daily 8-hr average ozone (MDA8 O_3) concentrations for July 2014. Panel (b) shows the six regions: northwest ("NW", orange), North China Plain ("NCP", red), northeast ("NE", green), southwest ("SW", purple), Pearl River Delta ("PRD", blue), and Yangtze River Delta ("YRD", yellow). Panel (c) shows the comparison between observed and simulated monthly mean ozone peak concentrations in the cities, and the data are color-coded by region. The horizonal and vertical bars denote the observed and simulated standard deviations, respectively. The red solid line corresponds to 1:1, and the red dashed lines are for 1:2 and 2:1. Panel (d) is the same as (c) but for monthly mean ozone peak time. The red solid line corresponds to 1:1, and the red dashed lines correspond to 1-hr difference from the 1:1 line.

6 p.m. The simulated ozone peak time data in 150 cities lie within 1 hr of the observed ozone peak time. The cities in the NCP region tend to have late afternoon (3 to 6 p.m.) ozone peaks while the cities in the PRD region tend to have early afternoon (1 to 4 p.m.) ozone peaks.

The regional day-to-day variability of observed and simulated data is also compared for ozone peak concentration (Figure S3) and peak time (Figure S4), and the overall time series is illustrated in Figure S5. The

Table 1
Statistics of Observed and Simulated Means and Standard Deviations (ppbv) of MDA8 Ozone in Six Regions for July 2014

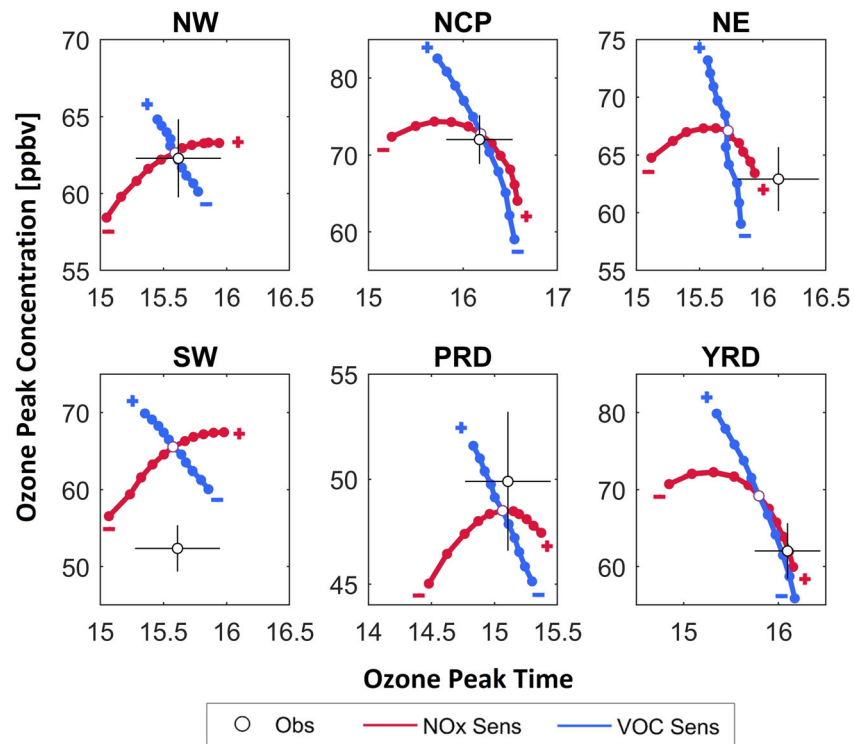|	NCP	NE	NW	PRD	YRD	SW	Overall
Observations	64 ± 9	56 ± 9	55 ± 11	41 ± 11	52 ± 8	43 ± 12	53 ± 13
Simulations	64 ± 8	59 ± 9	55 ± 6	42 ± 6	58 ± 12	56 ± 14	57 ± 12
Correlation coefficient	0.61	0.78	0.72	0.81	0.62	0.67	0.72

Figure 3. Sensitivities of ozone daily peak concentration and peak time to VOCs and NO_X emissions in the six regions for July 2014. The black open circles and lines show the observed peak averages and the corresponding standard deviations. The open circles at the intersection of the red and blue lines denote the standard simulation results. The red lines with solid dots show the sensitivities to NO_X emissions ("NO_XSens"); the blue lines with solid dots show the sensitivities of VOC emissions ("VOC Sens"). The signs of "+" and "−" denote an increase and decrease of the precursor emission in the model, respectively. Each dot denotes an increment or decrement of 10% in emissions. Sensitivities up to plus or minus 50% are shown.

ozone peak concentration data show high correlations between the observations and simulation results, indicating that the model can capture the day-to-day variance of the ozone peak concentrations reasonably well. However, the correlation between the observed and simulated ozone peak time is low. The low correlation is due in part to the small daily ozone peak variation in a region since the square of *R* is inversely proportional to the total sum of the data variance. For the overall time series. The median of the difference between the simulated and observed ozone peak time is 0.14 hr.

The observed and simulated daytime (10 a.m. to 4 p.m.) NO_2 concentrations are compared in Figures S6 and S7. The correlation coefficient between observed and simulated NO_2 is 0.56 for city-to-city variability and 0.43 for day-to-day variability, respectively. The day-to-day variability is higher (0.58–0.85) in the NCP, NE, PRD, and YRD regions and lower (0.48) in the NW and SW regions. Previous studies have shown that the surface measurements of NO_2 have high biases due to the interferences of other reactive nitrogen species such as peroxyacetyl nitrate (PAN) and nitric acid (HNO_3) and suggested a correction factor of 0.5 to the observation data in July in the United States (Lamsal et al., 2008; R. Zhang et al., 2018). However, in China, a ratio of 0.80 has been found between the satellite-derived surface NO_2 and CNEMC measurements in July (Gu et al., 2017). In this research, the ratio between the simulated and observed averaged NO_2 is 0.72, similar to Gu et al. (2017). Given the much shorter lifetime of NO_X than ozone in the summer, surface measurements of the former can be strongly affected by nearby local sources. The general lack of spatial representativeness of urban NO_2 measurements also contributes to the differences between observed and simulated surface NO_2 concentrations.

To further investigate the relationships of ozone peak concentration and time with NO_X and VOC emissions, we conduct two series of sensitivity tests: (1) NO_X emissions changing from − 50% to + 50% with an
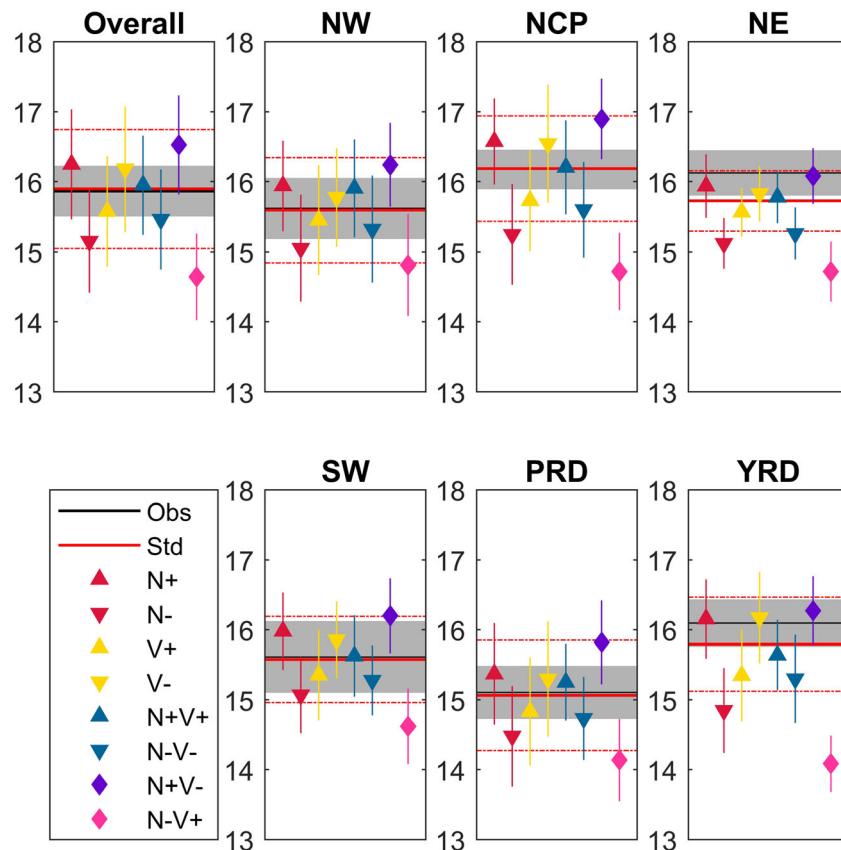
Figure 4. The sensitivities of simulated ozone peak time to NO_X and VOC emissions for July 2014. $N+$: increase NO_X emissions by 50%; $N-$: decrease NO_X emissions by 50%; $V+$: increase VOC emissions by 50%; $V-$: decrease VOC emissions by 50%; $N+V+$: increase both NO_X and VOC emissions by 50%; $N-V-$: decrease both NO_X and VOC emissions by 50%; $N+V-$: increase NO_X emissions by 50% and decrease VOC emissions by 50%; and $N-V+$: decrease NO_X emissions by 50% and increase VOC emissions by 50%.

increment of 10% and (2) VOC emissions changing from -50% to $+50\%$ with an increment of 10%. Figure 3 shows the monthly mean results of the sensitivity simulations in comparison with the observations. VOC emissions enhance the ozone peak concentration nearly linearly, while the NO_X emissions affect the ozone peak concentration differently. In the NW and SW regions, the ozone peak concentration increases with NO_X emissions, but the sensitivity decreases with increasing NO_X emissions. The peak ozone and NO_X emission relationship is no longer monotonic in the other four regions. While increasing NO_X emissions decrease the ozone peaks, decreasing NO_X emissions eventually also decrease the ozone peaks, but the turnover points are shifted to the left in the NCP, YRD, and NE regions. The sensitivity results of the ozone concentration to the emissions agree with previous studies (Li et al., 2013; Xing et al., 2011).

In contrast to the complex ozone peak concentration sensitivities to NO_X emissions, the sensitivities of ozone peak time to NO_X and VOC are monotonic. Increasing NO_X emissions delays the ozone peak time while increasing VOC emissions advances the ozone peak time in all six regions. For the same 50% change of emissions, the effect of NO_X is larger than VOCs, which partly explains the higher correlation coefficient between ozone peak time and NO_X emissions than those between ozone peak time and VOC emissions or for ozone peak concentration.

The monotonic sensitivities of ozone peak time to NO_X and VOC emissions compared to the more complex response of ozone peak concentration to emissions imply that the observations of ozone peak time provide good constraints on model simulations other than the observations of ozone peak concentration. It is only because the ambient ozone standard is based on concentrations that the observations of ozone peak time are usually not applied to evaluate model simulations. A further useful property of the simulated ozone
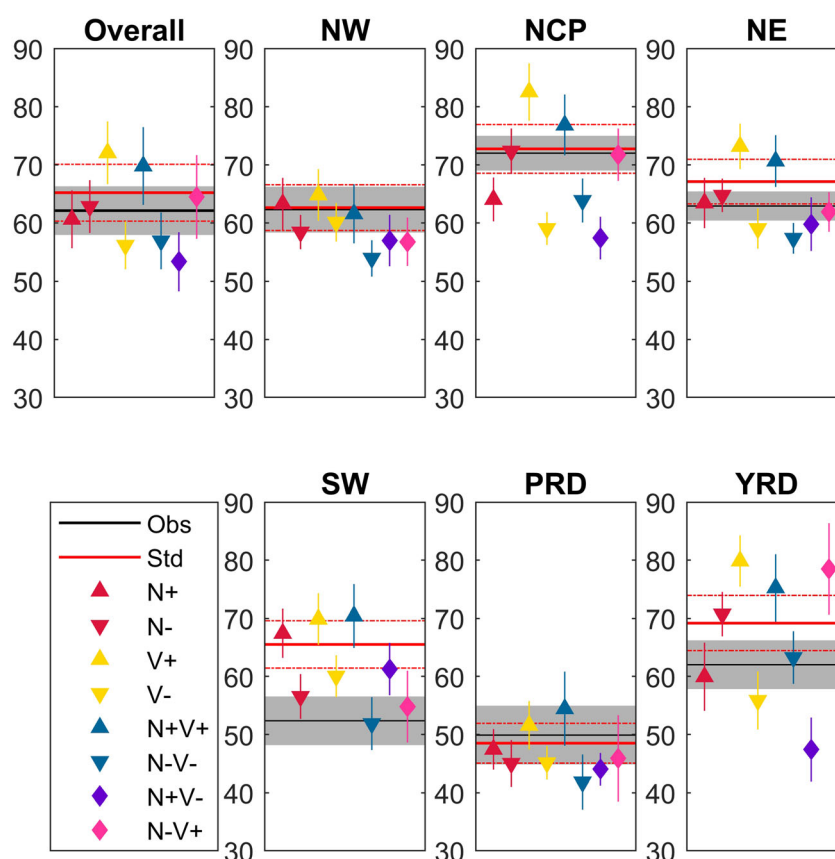
Figure 5. The same as Figure 4 but for ozone peak concentration.

peak time is that the impact of changing NO_X and VOC emissions concurrently by 50% is nearly additive (Figure 4): The change of ozone peak time in a simulation of changing NO_X and VOC emissions by 50% concurrently is close to the sum of the simulated changes of changing NO_X or VOC emissions by 50% alone. This additive effect does not exist in the ozone peak concentration simulations due to chemical nonlinearity (Figure 5), suggesting that the observed and simulated sensitivities of ozone peak time are easier to interpret than ozone peak concentration in urban regions of China.

We examine in more detailed chemical processes leading to these sensitivity results. The chemical production of ozone is due to the oxidation of NO by the hydroperoxy (HO_2) radicals or organic peroxy (RO_2) radicals. Peroxy radicals are mostly produced from the reactions of VOCs with OH. Photolysis of oxygenated VOCs (OVOCs) is also a large primary source of peroxy radicals in polluted urban regions. The reaction of OH with NO_2 is a large sink of radicals and NO_X (Liu et al., 2012). The sensitivities of OH, $HO_2 + RO_2$, and NO_X and the rates of OVOC photolysis, the reaction rate of OH and NO_2, and chemical production rate of O_3 (pO_3) to 50% changes of NO_X or VOCs are shown in Figure 6. The sensitivity results show that NO_X and VOC emissions affect ozone peak concentration and peak time in different ways. A 50% increase of NO_X emissions increases the radical sink through the reaction of OH and NO_2, suppressing radical concentrations. The net effect is a decrease in ozone production and peak ozone concentration. A 50% decrease of NO_X emissions has the opposite consequence. The radical suppressing effect by an increase of NO_X is larger in the early morning when the primary radical source is smaller than at noon. As a result, the ramping up of ozone production is delayed, and the ozone peak time is later. A 50% increase of VOC emissions increases HO_2 and RO_2 concentrations but does not affect NO_X concentrations as much, thereby increasing ozone production and peak concentrations. The effect of VOC emissions on ozone peak time is largely due to the reactions of the VOCs with the OH radical (Figure S8) and the photolysis of OVOCs, both of which peak before or at noon, while ozone peak time is in midafternoon (Figure 3). A 50% increase of VOC emissions increases
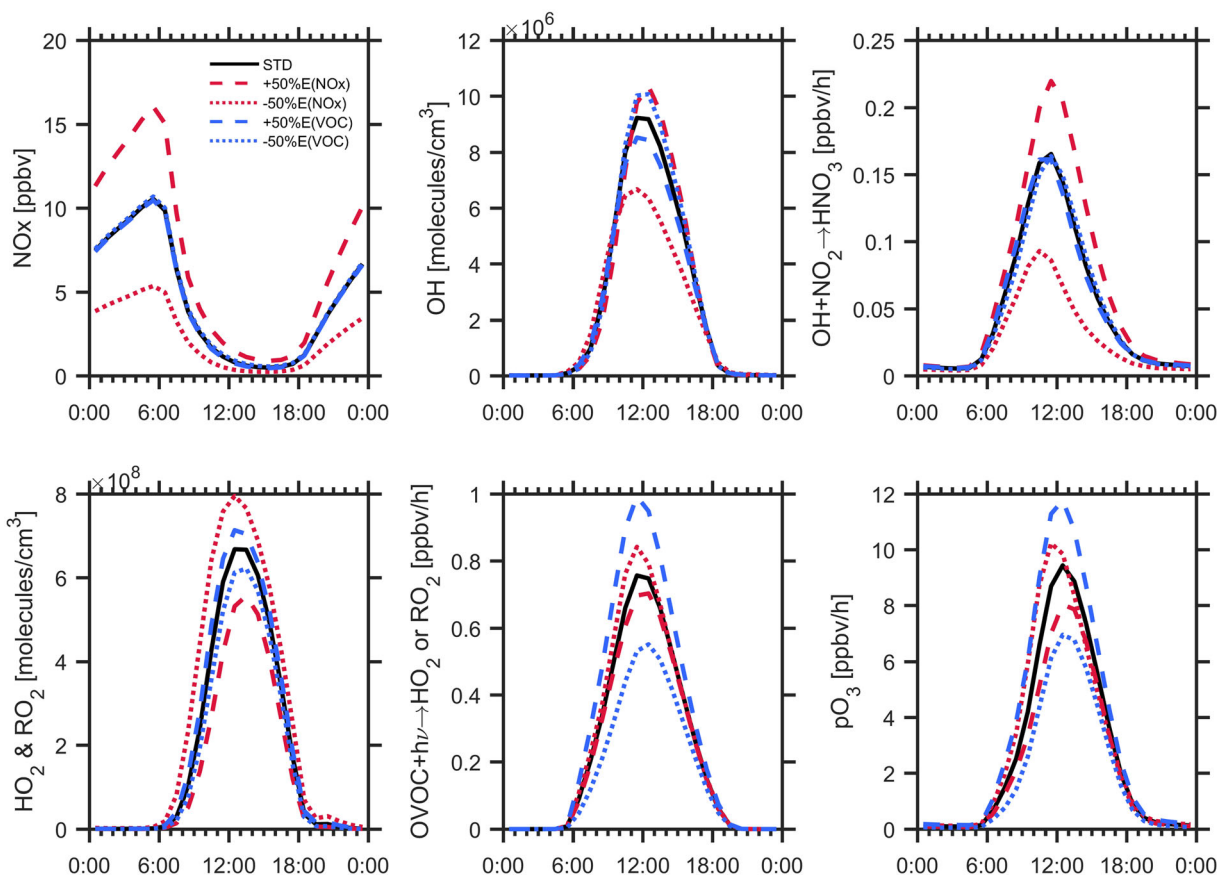
Figure 6. Sensitivities of OH, $HO_2 + RO_2$, NO_X, and the rates of OVOC photolysis, the reaction rate of OH and NO_2, and pO_3 to 50% changes of NO_X or VOCs at urban sites in this study for July 2014. The black lines are the results from the standard model; the red dashed lines show the results from a 50% increase of NO_X emissions; the red dotted lines show the results from a 50% decrease of NO_X emissions; the blue dashed lines show the results from a 50% increase of VOCs emissions; the blue dotted lines show the results from a 50% decrease of VOCs emissions.

OVOC photolysis, shifting HO_2 and RO_2 concentration peak toward noon and making ozone peak time occurs in earlier afternoon. Similarly, a 50% decrease of VOC emissions delays ozone peak time.

3.3. Isopleth Diagram for Ozone Peak Time

The EKMA isopleth diagram for the sensitivity of ozone to NO_X and VOC emissions has been widely used (Ashok & Barrett, 2016; Kinosian, 1982; Sillman et al., 1990; Sillman & Samson, 1993; Tan et al., 2018). We use the 0-D box model to compute the EKMA-type diagrams for ozone peak concentration and time for the urban regions of China in this study. Averaged hourly regional transport time, deposition rates, background concentrations, wind speed, and boundary layer height are included to simulate the effect of advection, mixing, and deposition. The results provide qualitative guidance on understanding the 3-D model results discussed previously.

Figure 7a shows the sensitivity diagrams for peak ozone concentration. The peak ozone sensitivity diagram is as expected. Under high NO_X and low VOC emissions, peak ozone concentration increases with increasing VOC and decreasing NO_X emissions, although the VOC sensitivity is much higher than NO_X. Hence, it is often referred to as the VOC-limited regime. Under low NO_X and high VOC emissions, which is often referred to as the NO_X-limited regime, peak ozone concentration increases with increasing NO_X emissions rapidly but is insensitive to VOC emissions. In the transition regime (near the area between the two dashed red lines in Figure 7), peak ozone concentration increases with increasing NO_X or VOC emissions. If the VOC to NO_X emission ratio (C:N ratio) decreases to the lower right of the diagram, the sensitivity of peak
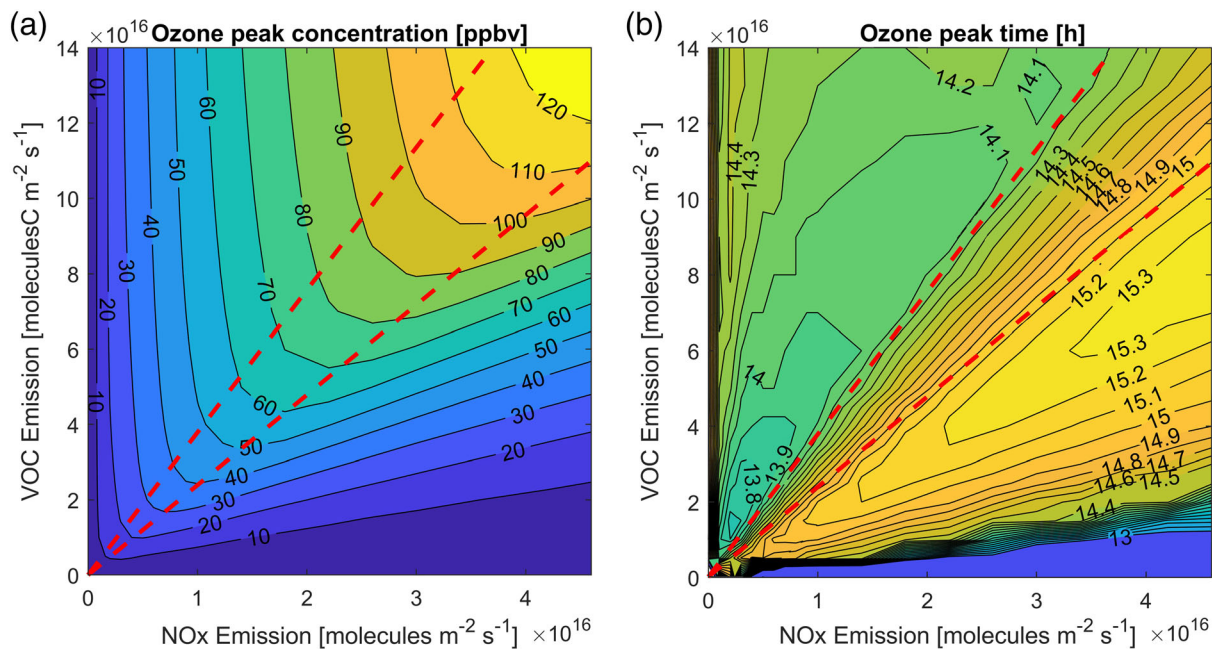
Figure 7. EKMA-type diagrams for the sensitivities of ozone peak concentration and time reacting to NO_X and VOC emissions simulated in the box model. The range of NO_X and VOC emission increments covers up to three times of average urban emissions in model grid cells with urban surface ozone observations. The red dashed lines bounding the transition regime are drawn based on the gradient of ozone peak time sensitivity to NO_X or VOC emissions, illustrating the different sensitivities of ozone peak time and concentrations to NO_X and VOC emissions.

ozone concentration to VOC emissions increases while the sensitivity of peak ozone concentration to NO_X emissions turns from positive to negative.

On average, the urban regions in China fall into the transition regime: the behaviors of the ozone peak concentrations in the NW and SW regions are centered in the transition regime while the other regions lean toward the side of the transition regime with lower VOC to NO_X (C:N) emission ratios. Figure 7b shows that the sensitivity of ozone peak time in the vicinity of the transition regime is quite consistent and nearly linear in comparison to the changing ozone peak concentration sensitivity in this regime. Increasing NO_X emissions or decreasing VOC emissions delays ozone peak time, in qualitative agreement with 3-D model simulation results. The reasons can be understood in Figure 6. For polluted urban regions, increasing NO_X emissions or decreasing VOC emissions has a similar effect of shifting the peak of peroxy radicals toward the afternoon and resulting in a later peak time of ozone. The former is due to an increase of the primary radical loss through the reaction of OH and NO_2, and the latter is due to a decrease of the primary radical source through the photolysis of OVOCs. As the C:N emission ratio continues decreasing to be <2:1 (lower right), ozone peak time is moved earlier by increasing NO_X emissions as peak ozone concentration decreases, while it is delayed by increasing VOC emissions as peak ozone concentration increases. In this regime, OH, ozone production, and chemical reactivity become increasingly suppressed by the reaction of OH and NO_2. Increasing VOC emissions decreases the effect of the reaction of OH and NO_2 since the fraction of OH reacts with VOCs would increase, and decreasing NO_X has a similar effect. When the C:N emission ratio continues to increase from the transition regime to the NO_X-limited regime in the upper left, ozone peak time becomes less sensitive to NO_X and VOC emission. In the highly enriched VOC emission regime, the peroxy radicals are not as sensitive to NO_X emissions as in the transition or VOC-limited regime.

The EKMA isopleth diagram first proposed by Kinosian (1982) is an important analysis method to diagnose the effectiveness of ozone precursor emission controls based on model simulations of the observation data. As such the applications of this analysis method in the original 0-D modeling framework need to target polluted regions where ozone peak values are controlled by local emissions while taking into account the uncertainties of the chemical mechanisms, boundary layer mixing, and emissions (e.g., National Research Council, 1991). In this work, we extend the sensitivities of ozone to precursor emissions to ozone peak

hour because of the additional information that can be garnered from the observations. The considerations for the applications of EKMA diagram also apply to our extension of the EKMA diagrams. We aggregated the ozone data on a regional basis (Figure 2) to reduce the uncertainties associated with local emissions, transport, and the limited data set size for a given city. When used in this manner, the extended EKMA diagram method can be applied to 3-D model simulation results to evaluate the model simulations and diagnose possible biases in the model emissions. The regional aggregation is effective for China because of the high density of polluted cities.

3.4. Diagnosing Potential Regional Emission Biases

The extended ozone-precursor relationships of Figure 7 can be applied to understand the implications of the observed changes in ozone peak time and concentration. For example, we would expect to see corresponding changes when urban emissions of NO_X or VOCs in a region decrease due to air quality control measures. The qualitative diagrams of Figure 7 provide quick guidance on the effectiveness of the control measures, and quantitative assessments can be carried out with modeling results (Figure 3). Here we illustrate the use of Figure 3 to understand potential problems in the emissions of NO_X or VOCs in the model. More detailed analysis is recommended particularly with respect to more thoroughly understanding the model uncertainties. Figure 3 shows that the simulation results are very close to the observations for the NW and NCP regions, implying good emission estimation, consistent with previous studies (Guo et al., 2019; Li et al., 2018). For the NE region, the model overestimates the observed ozone peak value and an early ozone peak time. To correct for both biases, the best solution is to increase NO_X by 50%. For the SW region, the ozone peak time is well simulated, but the ozone peak concentration is overestimated. The former dictates that a decrease of NO_X emissions must be accompanied by a decrease of VOC emissions since decreasing one alone would lead to a bias in simulated ozone peak time and reducing both emissions is optimal (Figure 5). Previous research suggested that MEIC may overestimate VOC emissions for 67% in Sichuan province in the SW region, consistent with our results (Zhou et al., 2019). For the PRD region, the model-observation difference is within the variability of the observed data. For the YRD region, the model estimates a higher peak concentration and an earlier peak time than the observations. These biases can be corrected by either increasing NO_X emissions or reducing VOC emissions. Since previous studies found overestimations of NO_X emission (Kong et al., 2019; Wu et al., 2017; L. Zhang et al., 2018; Zhang et al., 2020; Zhao et al., 2018), the simulation results of Figure 3 indicate that VOC emissions are also overestimated. The potential biases in the emissions discussed here need other methods such as direct measurements of NO_X and VOC concentrations or emissions to corroborate.

3.5. Uncertainty

For urban regions of China, Figure 7 qualitatively explains the additional information obtained by extending the ozone-precursor relationships from peak concentration to peak time. In and around the transition regime, ozone peak time is sensitive to both NO_X and VOC emissions, and its sensitivity to NO_X emissions is much more straightforward than that of peak ozone concentration. There are uncertainties of using the ozone-precursor relationships, which apply for the previously established ozone peak concentration as well as ozone peak time discussed here. One caveat is that the observations of ozone are reported every hour. When comparing model results to the observations, hourly data are also used. However, our analysis shows that the uncertainty of the peak time due to the hourly sampled observation and corresponding model data is negligible for the large datasets in this study (Text S2). The precision of ozone peak time and concentration can be improved by increasing the observation frequency from every hour to every 10 min, which can be easily achieved with today's technology. The same frequency must also be used for model data.

There are other factors to be considered which introduce uncertainties (e.g., National Research Council, 1991). The standard deviation of the observed regional ozone peak concentrations is ~3 ppbv, similar to previous studies for longer periods (K. Li et al., 2019; Lu et al., 2019). The model-simulated ozone systematic uncertainties are difficult to assess due in part to nonlinear chemistry (Liu et al., 2012). For practical purposes, the update-to-date chemical mechanisms need to be used in modeling. Previous studies mostly focused on ozone peak concentrations. In Mexico City, diurnal patterns of NO_X and VOC emissions can affect ozone peak concentrations by up to 17% (Ying et al., 2009). If we remove the diurnal variations of NO_X and VOC emissions, the largest effects occur in the NCP, NE, and PRD, where ozone peak time is
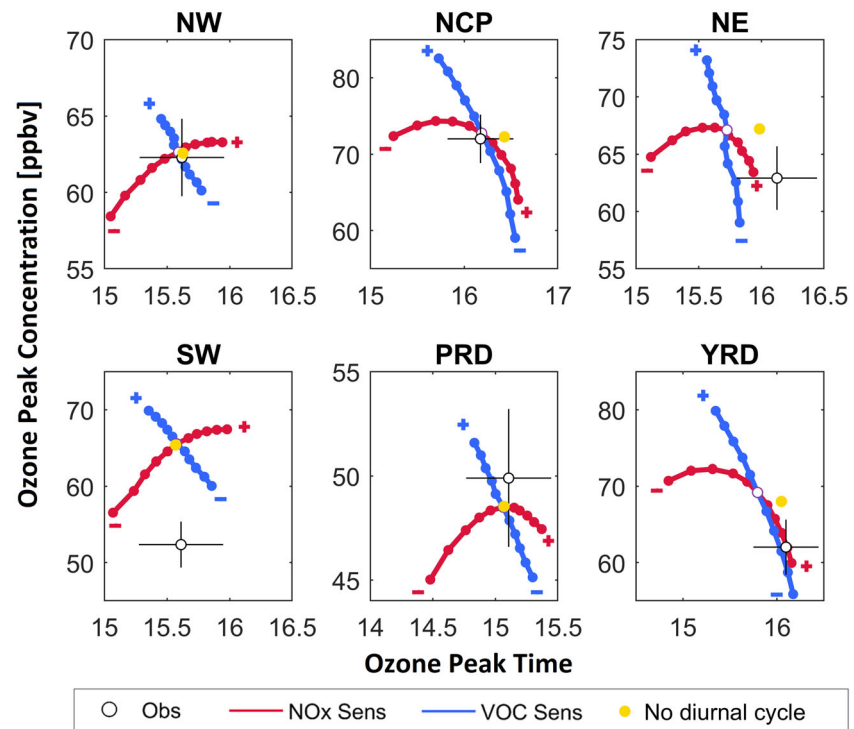
Figure 8. The same as Figure 3 with and extra case for removing the diurnal cycle of the emissions, marked as yellow dot.
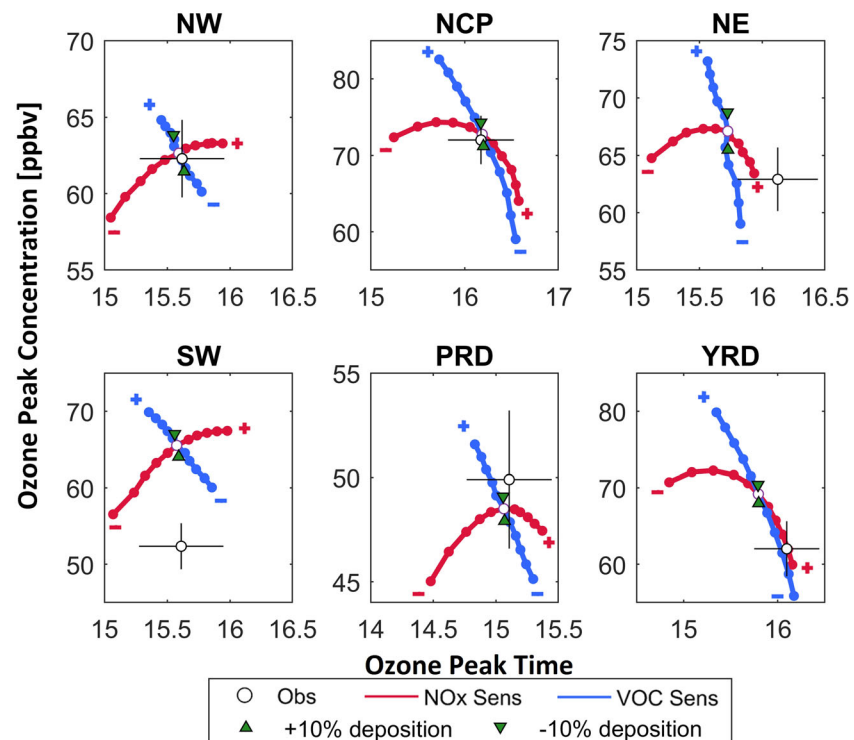

Figure 9. The same as Figure 3 with two extra cases for 10% enhancement and 10% reduction of the dry deposition rate of ozone, marked as green triangular pointing upward and downward, respectively.

delayed by ~0.25 hr, and ozone peak concentration decreases by 0.5 and 1 ppbv in NCP and YRD regions, respectively (Figure 8). The dry deposition also affects surface ozone (Zhao et al., 2019). Increasing or decreasing dry deposition rate by 10% does not affect simulated ozone peak time but changes ozone peak concentrations by up to 2 ppbv (Figure 9). Meteorology factors can also influence ozone concentrations (Hu et al., 2010; Lin et al., 2008), and dedicated studies are required. In general, the regional and monthly averages used in this study are less sensitive to meteorological biases than considering a single city.

4. Conclusions

In this study, we extend the ozone-precursor relationship to ozone peak time. The initial clue is simply based on the correlations of the observed ozone peak time and concentrations with NO_X and VOC emissions. We used the observations for the period of July 2014 to show that ozone peak time has better or comparable correlations with ozone precursor emissions in comparison to ozone peak concentration. It implies that the widely used EKMA diagram can be extended to observed ozone peak time and provides additional and independent constraints on ozone control strategies on the basis of widely available regulatory air quality monitoring data. We analyzed the observations for China, but the extended ozone-precursor relationships can be applied in other polluted regions where the EKMA diagram analysis is applicable.

We apply the 3-D REAM model with an extensive suite of sensitivity simulations to examine the sensitivities of ozone peak time and concentrations to NO_X and VOC emissions. The 3-D model sensitivity results are corroborated with the emission sensitivity isopleth diagram for ozone peak time similar to the EKMA diagram for ozone concentrations. The sensitivity distributions of ozone peak time and concentration differ significantly, indicating that the sensitivities of ozone peak time and concentration are complementary for regions with large anthropogenic emissions such as China. The ozone peak time is sensitive to both VOC and NO_X emissions, and the sensitivity is nearly linear in the transition regime of ozone production compared to the changing ozone peak concentration sensitivity in this regime, making the diagnostics of ozone peak time particularly valuable.

Since ozone is a secondary pollutant produced from photochemical reactions, the near-surface observations are not affected as much by heterogeneously distributed emission sources as NO_X and VOCs. The longer chemical lifetime of ozone than NO_X and fast-reacting VOCs also makes its measurements more representative than its precursors. Furthermore, the measurements of ozone are more reliable and readily available than NO_X and VOCs in China and other regions. The extended ozone-precursor relationships developed here provide both qualitative and quantitative constraints on understanding the effects on ozone by emission changes of NO_X and VOC. They can also be applied with air quality models to assess potential biases of NO_X and VOC emission inventories. In this work, we find that the emissions of ozone precursors are consistent with the observed ozone peak time and concentrations for the NW and NCP regions. In the NE region, NO_X emissions may have a low bias of 50%. In the SW region, both the NO_X and the VOC emissions are overestimated. In the YRD region, the VOC emissions are overestimated. In the PRD region, model results are in agreement with the observations within the uncertainties of the measurements. Such observation constraints on the basis of regulatory ozone observations can complement nicely the other measurement and modeling analysis methods for evaluating NO_X and the VOC emission inventories.

Before air quality models are applied to investigate effective strategies of controlling ozone precursor emissions, we suggest that the model simulations of ozone peak time and concentrations are evaluated using the extensive regulatory air quality monitoring network data in China. Model biases in simulated ozone peak time or concentrations provide important clues to potential model errors, such as systematic biases in the estimated emissions of ozone precursors. These biases in model simulations can lead to erroneous emission control strategies and need to be corrected before air quality models can be used in policy applications. The uncertainties of the method developed here are similar to previous studies using the EKMA diagram (Moore & Londergan, 2001; Tan et al., 2018). We examine specifically the uncertainties related to the diurnal variation of emissions and ozone dry deposition, and we find that they do not significantly affect the inference results of potential emission biases based on ozone observations. While not explicitly studied, the inference results are insensitive to short-term meteorology biases because the modeling analysis (e.g., Figures 3–9) is based on monthly and regional averaged results. Depending on the applications of the extended EKMA diagram analysis, further uncertainty analysis needs to be carried out.

Conflict of Interest

No conflict of interest is declared.

Data Availability Statement

The MEIC emission inventory can be accessed on the MEIC website (http://www.meicmodel.org/). The CNEMC data and the simulation data used in this research can be accessed online (https://doi.org/10.6084/m9.figshare.11860158.v4).

References

Ashok, A., & Barrett, S. R. H. (2016). Adjoint-based computation of U.S. nationwide ozone exposure isopleths. *Atmospheric Environment*, *133*, 68–80. https://doi.org/10.1016/j.atmosenv.2016.03.025

Bey, I., Jacob, D. J., Yantosca, R. M., Logan, J. A., Field, B. D., Fiore, A. M., et al. (2001). Global modeling of tropospheric chemistry with assimilated meteorology: Model description and evaluation. *Journal of Geophysical Research*, *106*, 23,073–23,095. https://doi.org/10.1029/2001JD000807

Blanchard, C. L., & Fairley, D. (2001). Spatial mapping of VOC and NO_X-limitation of ozone formation in central California. *Atmospheric Environment*, *35*, 3861–3873. https://doi.org/10.1016/S1352-2310(01)00153-4

CNEMC (2018). Monthly report on air quality of China cities. China National Environmental Monitoring Centre, http://www.cnemc.cn/jcbg/kqzlzkbg/201808/P020181010529659662339.pdf (in Chinese).

Duncan, B. N., Lamsal, L. N., Thompson, A. M., Yoshida, Y., Lu, Z., Streets, D. G., et al. (2016). A space-based, high-resolution view of notable changes in urban NO_X pollution around the world (2005–2014). *Journal of Geophysical Research: Atmosphere*, *121*, 976–996. https://doi.org/10.1002/2015JD024121

Gao, W., Tie, X., Xu, J., Huang, R., Mao, X., Zhou, G., & Chang, L. (2017). Long-term trend of O_3 in a mega city (Shanghai), China: Characteristics, causes, and interactions with precursors. *Science of Total Environment*, *603-604*, 425–433. https://doi.org/10.1016/j.scitotenv.2017.06.099

Geng, F., Tie, X., Xu, J., Zhou, G., Peng, L., Gao, W., et al. (2008). Characterization of ozone, NO_X, and VOCs measured in Shanghai, China. *Atmospheric Environment*, *42*(29), 6873–6883. https://doi.org/10.1016/j.atmosenv.2008.05.045

Gu, D., Wang, Y., Smeltzer, C., & Boersma, K. F. (2014). Anthropogenic emissions of NO_X over China: Reconciling the difference of inverse modeling results using GOME-2 and OMI measurements. *Journal of Geophysical Research: Atmosphere*, *119*, 7732–7740. https://doi.org/10.1002/2014JD021644

Gu, J., Chen, L., Yu, C., Li, S., Tao, J., Fan, M., et al. (2017). Ground-level NO_2 concentrations over China inferred from the satellite OMI and CMAQ model simulations. *Remote Sensing*, *9*(6), 519. https://doi.org/10.3390/rs9060519

Guenther, A. B., Jiang, X., Heald, C. L., Sakulyanontvittaya, T., Duhl, T., Emmons, L. K., & Wang, X. (2012). The Model of Emissions of Gases and Aerosols from Nature Version 2.1 (MEGAN2.1): An extended and updated framework for modeling biogenic emissions. *Geoscientific Model Development*, *5*, 1471–1492. https://doi.org/10.5194/gmd-5-1471-2012

Guo, H., Chen, K., Wang, P., Hu, J., Ying, Q., Gao, A., & Zhang, H. (2019). Simulation of summer ozone and its sensitivity to emission changes in China. *Atmospheric Pollution Research*, *10*, 1543–1552. https://doi.org/10.1016/j.apr.2019.05.003

Hu, X., Nielsen-Gammon, J. W., & Zhang, F. (2010). Evaluation of three planetary boundary layer schemes in the WRF model. *Journal of Applied Meteorology and Climatology*, *49*, 1831–1844. https://doi.org/10.1175/2010JAMC2432.1

Jimenez, P., & Baldasano, J. M. (2004). Ozone response to precursor controls in very complex terrains: Use of photochemical indicators to assess O_3-NO_X-VOC sensitivity in the northeastern Iberian Peninsula. *Journal of Geophysical Research*, *109*, D20309. https://doi.org/10.1029/2004JD004985

Jin, X., & Holloway, T. (2015). Spatial and temporal variability of ozone sensitivity over China observed from the Ozone Monitoring Instrument. *Journal of Geophysical Research: Atmosphere*, *120*, 7229–7246. https://doi.org/10.1002/2015JD023250

Karl, M., Walker, S., Solberg, S., & Ramacher, M. O. P. (2019). The Eulerian urban dispersion model EPISODE—Part 2: Extensions to the source dispersion and photochemistry for EPISODE-CityChem v1.2 and its application to the city of Hamburg. *Geoscientific Model Development*, *12*, 3357–3399. https://doi.org/10.5194/gmd-12-3357-2019

Kinosian, J. R. (1982). Ozone-precursor relationships from EKMA diagrams. *Environmental Science and Technology*, *16*(12), 880–883. https://doi.org/10.1021/es00106a011

Kong, H., Lin, J., Zhang, R., Liu, M., Weng, H., Ni, R., et al. (2019). High-resolution (0.05° × 0.05°) NO_X emissions in the Yangtze River Delta inferred from OMI. *Atmospheric Chemistry and Physics*, *19*, 12,835–12,856. https://doi.org/10.5194/acp-19-12835-2019

Lamsal, L. N., Martin, R. V., van Donkelaar, A., Steinbacher, M., Celarier, E. A., Bucsela, E., et al. (2008). Ground-level nitrogen dioxide concentrations inferred from the satellite-borne Ozone Monitoring Instrument. *Journal of Geophysical Research*, *113*, D16308. https://doi.org/10.1029/2007JD009235

Li, J., Wang, Y., & Qu, H. (2019). Dependence of summertime surface ozone on NO_X and VOC emissions over the United States: Peak time and value. *Geophysical Research Letters*, *46*, 3540–3550. https://doi.org/10.1029/2018GL081823

Li, K., Jacob, D. J., Liao, H., Shen, L., Zhang, Q., & Bates, K. H. (2019). Anthropogenic drivers of 2013–2017 trends in summer surface ozone in China. *Proceedings of the National Academy of Sciences of the United States of America*, *116*(2), 422–427. https://doi.org/10.1073/pnas.1812168116

Li, M., Zhang, Q., Korokawa, J., Woo, J., He, K., Lu, Z., et al. (2017). MIX: A mosaic Asian anthropogenic emission inventory under the international collaboration framework of the MICS-Asia and HTAP. *Atmospheric Chemistry and Physics*, *17*(2), 935–963. https://doi.org/10.5194/acp-17-935-2017

Li, N., He, Q., Greenberg, J., Guenther, A., Li, J., Cao, J., et al. (2018). Impacts of biogenic and anthropogenic emissions on summertime ozone formation in the Guanzhong Basin, China. *Atmospheric Chemistry and Physics*, *18*(10), 7489–7507. https://doi.org/10.5194/acp-18-7489-2018

Li, Y., Lau, A. K. H., Fung, J. C. H., Zheng, J., & Liu, S. (2013). Importance of NOX control for peak ozone reduction in the Pearl River Delta region. *Journal of Geophysical Research: Atmosphere*, *118*, 9428–9443. https://doi.org/10.1002/jgrd.50659

Lin, J., Da, P., & Zhang, R. (2013). Trend and interannual variability of Chinese air pollution since 2000 in association with socioeconomic development: A brief overview. *Atmospheric and Oceanic Science Letters*, *6*, 84–89. https://doi.org/10.1080/16742834.2013.11447061

Lin, J., Youn, D., Liang, X., & Wuebbles, D. J. (2008). Global model simulation of summertime U.S. ozone diurnal cycle and its sensitivity to PBL mixing, spatial resolution, and emissions. *Atmospheric Environment*, *42*, 8470–8483. https://doi.org/10.1016/j.atmosenv.2008.08.012

Liu, H., Liu, S., Xue, B., Lv, Z., Meng, Z., Yang, X., et al. (2018). Ground-level ozone pollution and its health impacts in China. *Atmospheric Environment*, *173*, 223–230. https://doi.org/10.1016/j.atmosenv.2017.11.014

Liu, Z., Wang, Y., Costabile, F., Amoroso, A., Zhao, C., Huey, L. G., et al. (2014). Evidence of aerosols as a media for rapid daytime HONO production over China. *Environmental Science and Technology*, *48*(24), 14,386–14,391. https://doi.org/10.1021/es504163z

Liu, Z., Wang, Y., Gu, D., Zhao, C., Huey, L. G., Stickel, R., et al. (2012). Summertime photochemistry during CAREBeijing-2007: RO_X budgets and O_3 formation. *Atmospheric Chemistry and Physics*, *12*(16), 7737–7752. https://doi.org/10.5194/acp-12-7737-2012

Liu, Z., Wang, Y., Vrekoussis, M., Richter, A., Wittrock, F., Burrows, J. P., et al. (2012). Exploring the missing source of glyoxal (CHOCHO) over China. *Geophysical Research Letters*, *39*, L10812. https://doi.org/10.1029/2012GL051645

Lu, X., Chen, N., Wang, Y., Cao, W., Zhu, B., Yao, T., et al. (2017). Radical budget and ozone chemistry during autumn in the atmosphere of an urban site in central China. *Journal of Geophysical Research: Atmosphere*, *122*, 3672–3685. https://doi.org/10.1002/2016JD025676

Lu, X., Hong, J., Zhang, L., Cooper, O. R., Schultz, M. G., Xu, X., et al. (2018). Severe surface ozone pollution in China: A global perspective. *Environmental Science and Technology Letters*, *5*(8), 487–494. https://doi.org/10.1021/acs.estlett.8b00366

Lu, X., Zhang, L., Chen, Y., Zhou, M., Zheng, B., Li, K., et al. (2019). Exploring 2016-2017 surface ozone pollution over China: Source contributions and meteorological influences. *Atmospheric Chemistry and Physics*, *19*(12), 8339–8361. https://doi.org/10.5194/acp-19-8339-2019

Ma, M., Gao, Y., Wang, Y., Zhang, S., Leung, L. R., Liu, C., et al. (2019). Substantial ozone enhancement over the North China Plain from increased biogenic emissions due to heat waves and land cover in summer 2017. *Atmospheric Chemistry and Physics*, *19*(19), 12,195–12,207. https://doi.org/10.5194/acp-19-12195-2019

Ma, Z., Xu, J., Quan, W., Zhang, Z., Lin, W., & Xu, X. (2016). Significant increase of surface ozone at a rural site, north of eastern China. *Atmospheric Chemistry and Physics*, *16*, 3969–3977. https://doi.org/10.5194/acp-16-3969-2016

Moore, G. E., & Londergan, R. J. (2001). Sampled Monte Carlo uncertainty analysis for photochemical grid models. *Atmospheric Environment*, *35*, 4863–4876. https://doi.org/10.1016/S1352-2310(01)00260-6

National Research Council (1991). *Rethinking the ozone problem in urban and regional air pollution*. Washington, DC: National Academic Press.

Ojha, N., Naja, M., Singh, K. P., Sarangi, T., Kumar, R., Lal, S., et al. (2012). Variabilities in ozone at a semi-urban site in the Indo-Gangetic Plain region: Association with the meteorology and regional processes. *Journal of Geophysical Research*, *117*, D20301. https://doi.org/10.1029/2012JD017716

Parra, M. A., Elustondo, D., Bermejo, R., & Santamaria, J. M. (2009). Ambient air levels of volatile organic compounds (VOC) and nitrogen dioxide (NO_2) in a medium-size city in Northern Spain. *Atmospheric Environment*, *407*, 999–1009. https://doi.org/10.1016/j.scitotenv.2008.10.032

Ran, L., Zhao, C., Geng, F., Tie, X., Tang, X., Peng, L., et al. (2009). Ozone photochemical production in urban Shanghai, China: Analysis based on ground level observations. *Journal of Geophysical Research*, *114*, D15301. https://doi.org/10.1029/2008JD010752

Ren, X., Duin, D., Cazorla, M., Chen, S., Mao, J., Zhang, L., et al. (2013). Atmospheric oxidation chemistry and ozone production: Results from SHARP 2009 in Houston, Texas. *Journal of Geophysical Research: Atmosphere*, *118*, 5770–5780. https://doi.org/10.1002/jgrd.50342

Saha, S., Moorthi, S., Wu, X., Wang, J., Nadiga, S., Tripp, P., et al. (2013). The NCEP Climate Forecast System Version 2. *Journal of Climate*, *27*(6), 2185–2208. https://doi.org/10.1175/JCLI-D-12-00823.1

Seinfeld, J. H., & Pandis, S. N. (2016). *Atmospheric chemistry and physics: From air pollution to climate change* (3rd ed.). New Jersey: John Wiley & Sons, Inc.

Sillman, S., Logan, J. A., & Wofsy, S. C. (1990). The sensitivity of ozone to nitrogen oxides and hydrocarbons in regional ozone episodes. *Journal of Geophysical Research*, *95*, 1837–1851. https://doi.org/10.1029/JD095iD02p01837

Sillman, S., & Samson, P. J. (1993). Nitrogen oxides, regional transport, and ozone air quality: Results of a regional-scale model for the Midwestern United States. *Water, Air, and Soil Pollution*, *67*(1–2), 117–132. https://doi.org/10.1007/BF00480817

Sun, L., Xue, L., Wang, Y., Li, L., Lin, J., Ni, R., et al. (2019). Impacts of meteorology and emissions on summertime surface ozone increases over central eastern China between 2003 and 2015. *Atmospheric Chemistry and Physics*, *19*(3), 1455–1469. https://doi.org/10.5194/acp-19-1455-2019

Tan, Z., Lu, K., Jiang, M., Su, R., Dong, H., Zeng, L., et al. (2018). Exploring ozone pollution in Chengdu, southwestern China: A case study from radical chemistry to O_3-VOC-NO_X sensitivity. *Science of Total Environment*, *636*, 775–786. https://doi.org/10.1016/j.scitotenv.2018.04.286

Tukey, J. W. (1977). *Exploratory Data Analysis*. United Kingdom: Addison-Wesley.

U.S. EPA (2013). Integrated science assessment for ozone and related photochemical oxidants. National Center for Environmental Assessment: RTP, NC, EPA/600/R-10/076F.

Wang, T., Xue, L., Brimblecombe, P., Lam, Y. F., Li, L., & Zhang, L. (2017). Ozone pollution in China: A review of concentrations, meteorological influences, chemical precursors, and effects. *Science of Total Environment*, *575*, 1582–1596. https://doi.org/10.1016/j.scitotenv.2016.10.081

Wang, W., Cheng, T., Gu, X., Chen, H., Guo, H., Wang, Y., et al. (2017). Assessing spatial and temporal patterns of observed ground-level ozone in China. *Scientific Reports*, *7*(1), 3651. https://doi.org/10.1038/s41598-017-03929-w

Wang, Y., Choi, Y., Zeng, T., Davis, D., Buhr, M., Huey, G. L., & Neff, W. (2007). Assessing the photochemical impact of snow emissions over Antarctica during ANTCI 2003. *Atmospheric Environment*, *41*(19), 3944–3958. https://doi.org/10.1016/j.atmosenv.2007.01.056

Wang, Y., Choi, Y., Zeng, T., Ridley, B., Blake, N., Blake, D., & Flocke, F. (2006). Late-spring increase of trans-Pacific pollution transport in the upper troposphere. *Geophysical Research Letters*, *33*, L01811. https://doi.org/10.1029/2005GL024975

Wu, J., Wang, Q., Chen, H., Zhang, Y., & Wild, O. (2017). On the origin of surface ozone episode in Shanghai over Yangtze River Delta during a prolonged heat wave. *Aerosol and Air Quality Research*, *17*, 2804–2815. https://doi.org/10.4209/aaqr.2017.03.0101

Xing, J., Wang, S. X., Jang, C., Zhu, Y., & Hao, J. M. (2011). Nonlinear response of ozone to precursor emission changes in China: A modeling study using response surface methodology. *Atmospheric Chemistry and Physics*, *11*, 5027–5044. https://doi.org/10.5194/acp-11-5027-2011

Xu, J., Zhang, Q., Shi, J., Ge, X., Xie, C., Wang, J., et al. (2018). Chemical characteristics of submicron particles at the central Tibetan Plateau: Insights from aerosol mass spectrometry. *Atmospheric Chemistry and Physics*, *18*(1), 427–443. https://doi.org/10.5194/acp-18-427-2018

Yang, G., Liu, Y., & Li, X. (2020). Spatiotemporal distribution of ground-level ozone in China at a city level. *Scientific Reports*, *10*(1), 7229. https://doi.org/10.1038/s41598-020-64111-3

Yang, Q., Wang, Y., Zhao, C., Liu, Z., Gustafson, W. I. Jr., & Shao, M. (2011). NO_X emission reduction and its effects on ozone during the 2008 Olympic games. *Environmental Science and Technology*, *45*(15), 6404–6410. https://doi.org/10.1021/es200675v

Ying, Z., Tie, X., & Li, G. (2009). Sensitivity of ozone concentrations to diurnal variations of surface emissions in Mexico City: A WRF/Chem modeling study. *Atmospheric Environment*, *43*, 851–859. https://doi.org/10.1016/j.atmosenv.2008.10.044

Zeng, T., Wang, Y., Chance, K., Blake, N., Blake, D., & Ridley, B. (2006). Halogen-driven low-altitude O_3 and hydrocarbon losses in spring at northern high latitudes. *Journal of Geophysical Research*, *111*, D17313. https://doi.org/10.1029/2005JD006706

Zhang, L., Zhao, T., Gong, S., Kong, S., Tang, L., Liu, D., et al. (2018). Updated emission inventories of power plants in simulating air quality during haze periods over East China. *Atmospheric Chemistry and Physics*, *18*(3), 2065–2079. https://doi.org/10.5194/acp-18-2065-2018

Zhang, R., Wang, Y., He, Q., Chen, L., Zhang, Y., Qu, H., et al. (2017). Enhanced trans-Himalaya pollution transport to the Tibetan Plateau by cut-off low systems. *Atmospheric Chemistry and Physics*, *17*(4), 3083–3095. https://doi.org/10.5194/acp-17-3083-2017

Zhang, R., Wang, Y., Smeltzer, C., Qu, H., Koshak, W., & Boersma, K. F. (2018). Comparing OMI-based and EPA AQS in situ NO2 trends: Towards understanding surface NO_X emission changes. *Atmospheric Measurement Techniques*, *11*, 3955–3967. https://doi.org/10.5194/amt-11-3955-2018

Zhang, R., Zhang, Y., Lin, H., Feng, X., Fu, T., & Wang, Y. (2020). NO_X emission reduction and recovery during COVID-19 in East China. *Atmosphere*, *11*, 433. https://doi.org/10.3390/atmos11040433

Zhang, Y., Wang, Y., Chen, G., Smeltzer, C., Crawford, J., Olson, J., et al. (2016). Large vertical gradient of reactive nitrogen oxides in the boundary layer: Modeling analysis of DISCOVER-AQ 2011 observations. *Journal of Geophysical Research: Atmosphere*, *121*, 1922–1934. https://doi.org/10.1002/2015JD024203

Zhao, B., Wang, S. X., Liu, H., Xu, J. Y., Fu, K., Klimont, Z., et al. (2013). NOx emissions in China: Historical trends and future perspectives. *Atmospheric Chemistry and Physics*, *13*(19), 9869–9897. https://doi.org/10.5194/acp-13-9869-2013

Zhao, C., Wang, Y., Choi, Y., & Zeng, T. (2009). Summertime impact of convective transport and lightning NO_X production over North America: Modeling dependence on meteorological simulations. *Atmospheric Chemistry and Physics*, *9*, 4315–4327. https://doi.org/10.5194/acp-9-4315-2009

Zhao, C., Wang, Y., & Zeng, T. (2009). East China plains: A "basin" of ozone pollution. *Environmental Science and Technology*, *43*(6), 1911–1915. https://doi.org/10.1021/es8027764

Zhao, Y., Xia, Y., & Zhou, Y. (2018). Assessment of a high-resolution NO_X emission inventory using satellite observations: A case study of southern Jiangsu, China. *Atmospheric Environment*, *190*, 135–145. https://doi.org/10.1016/j.atmosenv.2018.07.029

Zhao, Y., Zhang, L., Zhou, M., Chen, D., Lu, X., Tao, W., et al. (2019). Influences of planetary boundary layer mixing parameterization on summertime surface ozone concentration and dry deposition over North China. *Atmospheric Environment*, *218*, 116950. https://doi.org/10.1016/j.atmosenv.2019.116950

Zhou, Z., Tan, Q., Deng, Y., Wu, K., Yang, X., & Zhou, X. (2019). Emission inventory of anthropogenic air pollutant sources and characteristics of VOCs species in Sichuan Province, China. *Journal of Atmospheric Chemistry*, *76*(1), 21–58. https://doi.org/10.1007/s10874-019-9386-7